

# Diffusion and perfusion MR parameters to assess preoperative short-course radiotherapy response in locally advanced rectal cancer: a comparative explorative study among Standardized Index of Shape by DCE-MRI, intravoxel incoherent motion- and diffusion kurtosis imaging-derived parameters

Roberta Fusco,<sup>1</sup> Mario Sansone,<sup>2</sup> Vincenza Granata,<sup>1</sup> Robert Grimm,<sup>3</sup> Ugo Pace,<sup>4</sup> Paolo Delrio,<sup>4</sup> Fabiana Tatangelo,<sup>5</sup> Gerardo Botti,<sup>5</sup> Antonio Avallone,<sup>6</sup> Biagio Pecori,<sup>7</sup> and Antonella Petrillo<sup>1</sup>

<sup>1</sup>Division of Radiology, Istituto Nazionale Tumori - IRCCS - Fondazione G. Pascale, Via Mariano Semmola, 80131 Naples, Italy

<sup>2</sup>Department of Electrical Engineering and Information Technologies (DIETI), Via Claudio 21, 80125 Naples, Italy

<sup>3</sup>Siemens Healthcare GmbH, Erlangen, Germany

<sup>4</sup>Division of Gastrointestinal Surgical Oncology, Istituto Nazionale Tumori - IRCCS - Fondazione G. Pascale, Via Mariano Semmola, 80131 Naples, Italy

<sup>5</sup>Division of Diagnostic Pathology, Istituto Nazionale Tumori - IRCCS - Fondazione G. Pascale, Via Mariano Semmola, 80131 Naples, Italy

<sup>6</sup>Division of Gastrointestinal Medical Oncology, Istituto Nazionale Tumori - IRCCS - Fondazione G. Pascale, Via Mariano Semmola, 80131 Naples, Italy

<sup>7</sup>Division of Radiotherapy, Istituto Nazionale Tumori - IRCCS - Fondazione G. Pascale, Via Mariano Semmola, 80131 Naples, Italy

## Abstract

**Purpose:** To assess preoperative short-course radiotherapy (SCR) tumor response in locally advanced rectal cancer (LARC) by means of Standardized Index of Shape (SIS) by dynamic contrast-enhanced magnetic resonance imaging (DCE-MRI), apparent diffusion coefficient (ADC), intravoxel incoherent motion (IVIM) and diffusion kurtosis imaging (DKI) parameters derived from diffusion-weighted MRI (DW-MRI).

**Materials and methods:** Thirty-four patients with LARC who underwent MRI scans before and after SCR followed by delayed surgery, retrospectively, were enrolled. SIS,

ADC, IVIM parameters [tissue diffusion ( $D_t$ ), pseudo-diffusion ( $D_p$ ), perfusion fraction ( $f_p$ )] and DKI parameters [mean diffusivity (MD), mean of diffusional kurtosis (MK)] were calculated for each patient. IVIM parameters were estimated using two methods, namely conventional biexponential fitting (CBFM) and variable projection (VARPRO). After surgery, the pathological TNM and tumor regression grade (TRG) were estimated. For each parameter, percentage changes between before and after SCR were evaluated. Furthermore, an artificial neural network was trained for outcome prediction. Nonparametric sample tests and receiver operating characteristic curve (ROC) analysis were performed.

**Results:** Fifteen patients were classified as responders ( $TRG \leq 2$ ) and 19 as not responders ( $TRG > 3$ ). Seven patients had TRG 1 (pathological complete response,

pCR). Mean and standard deviation values of pre-treatment CBFM  $D_p$  and mean value of VARPRO  $D_p$  pre-treatment showed statistically significant differences to predict pCR. ( $p$  value at Mann–Whitney test was 0.05, 0.03 and 0.008, respectively.) Exclusively SIS percentage change showed significant differences between responder and non-responder patients after SCR ( $p$  value  $<< 0.001$ ) and to assess pCR after SCR ( $p$  value  $<< 0.001$ ). The best results to predict pCR were obtained by VARPRO  $F_p$  mean value pre-treatment with area under ROC of 0.84, a sensitivity of 96.4%, a specificity of 71.4%, a positive predictive value (PPV) of 92.9%, a negative predictive value (NPV) of 83.3% and an accuracy of 91.2%. The best results to assess after treatment complete pathological response were obtained by SIS with an area under ROC of 0.89, a sensitivity of 85.7%, a specificity of 92.6%, a PPV of 75.0%, a NPV of 96.1% and an accuracy of 91.2%. Moreover, the best results to differentiate after treatment responders vs. non-responders were obtained by SIS with an area under ROC of 0.94, a sensitivity of 93.3%, a specificity of 84.2%, a PPV of 82.4%, a NPV of 94.1% and an accuracy of 88.2%. Promising initial results were obtained using a decision tree tested with all ADC, IVIM and DKI extracted parameter: we reached high accuracy to assess pathological complete response after SCR in LARC (an accuracy of 85.3% to assess pathological complete response after SCR using VARPRO  $D_p$  mean value post-treatment, ADC standard deviation value pre-treatment, MD standard deviation value post-treatment). **Conclusion:** SIS is a hopeful DCE-MRI angiogenic biomarker to assess preoperative treatment response after SCR with delayed surgery. Furthermore, an important prognostic role was obtained by VARPRO  $F_p$  mean value pre-treatment and by a decision tree composed by diffusion parameters derived by DWI and DKI to assess pathological complete response.

**Key words:** LARC—Short-course radiotherapy—Response assessment—Standardized Index of Shape—IVIM-derived parameters—DKI-derived parameters

### Abbreviations

AUC	Area under ROC curve
CTV	Clinical target volume
CT	Computed tomography
CBFM	Conventional biexponential fitting
DCE-MRI	Dynamic contrast-enhanced magnetic resonance imaging
DWI	Diffusion-weighted imaging
DKI	Diffusion kurtosis imaging
$D_t$	Tissue diffusion

$D_p$	Pseudo-diffusion
$f_p$	Perfusion fraction
IMRT	Intensity-modulated radiation therapy
IVIM	Intravoxel incoherent motion
LARC	Locally advanced rectal cancer
MD	Mean diffusivity
MK	Mean of diffusional kurtosis
MLC	Multileaf collimators
MSD	Maximum signal difference
NPV	Negative predictive value
pCR	pathological complete response
pCRT	Preoperative chemo-radiation therapy
PPV	Positive predictive value
ROC	RECEIVER operating characteristic
ROI	Regions of interest
SCR	Short-course radiotherapy
SCRDS	Short-course radiotherapy with delayed surgery
SIS	Standardized Index of Shape
TRG	Tumor regression grade
WOS	Washout slope
VARPRO	Variable projection
VOI	Volume of interest

Total mesorectal excision combined with preoperative radiation therapy and chemotherapy (pCRT) is the current standard for locally advanced rectal cancer (LARC) [1–3]. Long-course CRT has been extensively applied, and encouraging results derive from this approach in terms of local control with a high percentage of tumor regression up to a significant rate of complete response [1–3]. However, short-course radiotherapy (SCR) is known to be a valuable therapeutic option in patients with LARC. A recent meta-analysis [4] reported that SCR with immediate surgery is as effective as long CRT with deferred surgery in terms of overall and disease-free survival rates, local and distant control and toxicity. Also, short-course radiotherapy with delayed surgery (SCRDS) (after 4–8 weeks), optional therapy described for patients with locally advanced tumors who are not fit for CRT, leads to similar results in terms of negative margin resection percentage and satisfactory results about the downstaging and pathological response rate compared to traditional pCRT [5–13].

The use of new imaging modalities to make individual assessments of therapy response could be of great clinical value to adjust subsequent strategies tailored for each patient. Such strategies range from a tailored surgical approach, to administering an adjuvant regimen, or even to a wait-and-see policy without surgery for patients with high surgical risks [14, 15].

A positive tumor response does not necessarily require a significant tumor size reduction in morphological MRI [16]; there is difficulty to differentiate necrosis, fibrotic tissue and viable residual tumor tissue within treated areas [16, 17]. Several studies focused their attention on the potential added benefit of functional quantitative parameters derived by MR image [17–20]. Dynamic contrast-enhanced MRI (DCE-MRI) has demonstrated promise to detect residual tumor after pre-surgery CRT [17–21]. Previous studies have investigated functional parameters derived from DCE-MRI data in rectal cancer [18–21] such as the Standardized Index of Shape proposed by Petrillo et al. [18] as a simple semi-quantitative parameter capable to differentiate pathological significant and complete response after CRT in LARC and after SCRDS [22]. Moreover, in various oncology fields, researchers have recommended the use of diffusion-weighted imaging (DWI) to assess treatment response [23–30]. DWI provides functional information on the tissues' microstructure by means of the evaluation of water proton mobility differences [23, 24]. Water diffusion characteristics depend on cell density, vascularity, viscosity of the extracellular fluid and cell membrane integrity. By quantifying these properties by means of the individual apparent diffusion coefficient (ADC) using a monoexponential model to analyze DWI data, it can be used as an imaging biomarker to reflect biologic tumor changes and to monitor and predict treatment response [25, 26]. Moreover, using a biexponential model to analyze DWI data, information on both diffusion and perfusion tissue properties derived from intravoxel incoherent motion method (IVIM) can be obtained: the pure tissue coefficient ( $D_t$ ) that describes water macroscopic motion in the cellular interstitial space, the pseudo-diffusion coefficient ( $D_p$ ) that describes blood microscopic motion in the vessels, and the perfusion fraction ( $f_p$ ) that describes the proportion of the two different motions [27–30].

Also, the conventional DWI model is based on the assumption that water diffusion within a voxel has a single component and follows a Gaussian behavior where water molecules diffuse without any restriction [31]. However, due to the presence of microstructures (i.e., two tissue types or components within one voxel, and organelles and cell membranes), random motion or diffusion of thermally agitated water molecules within biologic tissues exhibits non-Gaussian behavior [32]. Jensen and co-workers in 2005 proposed a non-Gaussian diffusion model called diffusion kurtosis imaging (DKI) [32]. This model includes the kurtosis coefficient ( $K$ ), that measures the deviation of tissue diffusion from a Gaussian model, and the diffusion coefficient ( $D$ ) with the correction of non-Gaussian bias.

Aim of this study is to determine the diagnostic performance of MR imaging for the assessment of tumor response after SCRDS in patients with LARC using

Standardized Index of Shape (SIS) obtained by DCE-MRI, using ADC-, IVIM- and DKI-derived parameters obtained by DW-MRI. A multivariate analysis of all functional MR-derived parameters extracted by DCE- and DW-MRI using a neural network was also evaluated.

## Materials and methods

### *Patient selection*

Thirty-four patients with a median age of 67 years (range 48–83 years) who refused or were considered unfit for chemo-radiation and planned for neoadjuvant short-course radiotherapy were evaluated in this retrospective study, from May 2011 to December 2016.

Patient characteristics are described in Table 1.

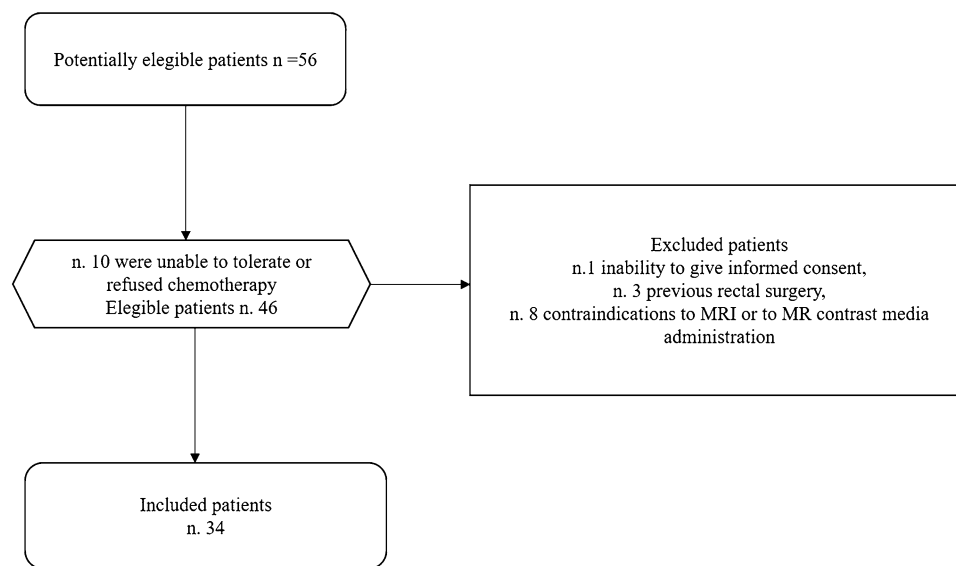
All patients had a biopsy-proven rectal adenocarcinoma. Endorectal ultrasonography, MRI of pelvis and computed tomography (CT) scan of chest, abdomen and pelvis were used as staging examinations. Patients who had T2 with local lymph node involvement, T3 rectal cancer with or without local lymph node involvement and patient with T4 were included. Exclusion criteria were: inability to give informed consent, previous rectal surgery and contraindications to MRI or to MR contrast media administration (see Fig. 1). Patients were included in the study in accordance with the approved guidelines of ethical committee of National Cancer Institute of Naples and gave their written informed consent.

### *Radiotherapy*

All patients underwent dose-planning CT in prone position. After an online CT virtual simulation, CT datasets were transferred to a dedicated treatment planning system through a DICOM network, and an individualized clinical target volume (CTV) was done, including the gross tumor volume with margins (2–3 cm depending upon tumor position, defined by MRI imaging), the mesorectum and regional lymph nodes depending upon tumor location. We contoured the small bowel, the femoral heads and the bladder as critical organs on all CT slices of every patient, and we evaluated the relative dose–volume histogram on the treatment planning console. Three-dimensional plans for 3D or intensity-modulated radiation therapy (IMRT) radiotherapy were generated for a dual-energy, 6–20 MV X-ray linear accelerator (Clinac 2100, Varian Medical Systems, Palo Alto, CA) or for a 6–15 MV X-ray linear accelerator (Elekta Agility, Elekta Instrument AB Stockholm, Stockholm, Sweden), both equipped with multileaf collimators (MLC). Patients were scheduled using a 3-field or IMRT treatment arrangement to include the planning target volume within the 95% isodose, and a dose of 25 Gy in 5 fractions over 1 week was prescribed to the

**Table 1.** Patient characteristics and histopathological findings

Characteristics	All patients <i>n</i> = 34 (%)	TRG 1–2 <i>n</i> = 15	TRG 3–4 <i>n</i> = 19	<i>p</i> *
Gender				> 0.05
Male/female	26(76.5)/8(23.5)	10/5	16/3	
Median age (range)	67(48–83)	69(48–78)	68(48–76)	
Gunderson risk				> 0.05
Intermediate: T3N0, T2N1	8(23.5)	3	5	
Moderately high: T2N2, T3N1, T4N0	17(50.0)	7	10	
High: T3N2	9(26.5)	5	4	
Distance from the anal verge				> 0.05
≤ 5 cm	14(41.2)	6	8	
> 5 cm	20(58.8)	9	11	
Circumferential resection margin				> 0.05
> 2 mm	15(44.1)	6	9	
≤ 2 mm	13(38.2)	6	7	
≤ 1 mm	5(14.7)	2	3	
Not measurable	1(2.9)	0	1	

**Fig. 1.** Flowchart showing how patients were included in the study.

ICRU 62 intersection point. Surgery was performed 5(±1) weeks on average after the end of radiotherapy.

### MRI data acquisitions

Each patient underwent MR studies before and after SCR: baseline, on average 23.8 days (9 days of standard deviation) before starting radiotherapy, and delayed, on average 61.0 days (11 days of standard deviation) after the end of SCR.

DCE-MRI was performed with a 1.5T scanner (MAGNETOM Symphony, Siemens Healthcare, Erlangen, Germany) and phased-array body coil. Pre-contrast coronal T1-weighted 2D turbo spin-echo (TSE) images, sagittal and axial T2w 2D TSE images were acquired. Axial DW images were obtained with a single-shot spin-echo diffusion-weighted echo-planar pulse sequence (SE-DW-EPI) at *b* values of 0, 50, 100, 150, 300, 600, 800 s/

mm<sup>2</sup>. Axial dynamic contrast-enhanced T1-weighted FLASH 3D gradient-echo images were obtained: one sequence before and ten sequences after intravenous injection of 0.1 mmol/kg of a positive, gadolinium-based paramagnetic contrast agent (Gd-DOTA, Dotarem, Guerbet, Roissy-CdG-Cedex, France) at 2 mL/s of flow rate, followed by a 10-mL saline flush at the same rate. Sagittal, axial and coronal post-contrast T1-weighted 2D TSE images with and without fat saturation were also acquired. Table 2 reports MR sequence parameters. In order to reduce respiratory artefacts, each patient received bowel preparation and antispasmodic medication.

### MRI image data analysis

Image assessment was performed in a single reading session for each patient by consensus of two gastrointestinal radiologists with 25 years and 10 years of expe-

**Table 2.** Pulse sequence parameters on MR studies

Sequence	Orientation	TR/TE/FA (ms/ms/deg.)	FOV (mm × mm)	Pixel spacing	ST/gap (mm/mm)
T1w 2D TSE	Coronal	499/13/150	450 × 450	0.87 × 0.87	3/0
T2w 2D TSE	Sagittal	4820/98/150	250 × 250	0.78 × 0.78	3/0
T2w 2D TSE	Axial	3970/98/150	250 × 250	0.78 × 0.78	3/0
SE-DW-EPI	Axial	2700/83	270 × 230	1.70 × 1.70	4/0
T1w FLASH 3D	Axial	9.8/4.76/25	330 × 247	0.59 × 0.59	3/0
T1w FLASH 3D	Axial	9.8/4.76/25	330 × 247	0.59 × 0.59	3/0
T1w 2D TSE	Sagittal	538/13/150	250 × 250	0.48 × 0.48	3/0
T1w 2D TSE	Coronal	538/13/150	250 × 250	0.48 × 0.48	3/0
T1w 2D TSE	Axial	450/12/150	270 × 236	0.52 × 0.52	3/0

TR, repetition time; TE, echo time; FOV, field of view; FA, flip angle; ST, slice thickness; TF, turbo factor; AT, acquisition time

rience in reading pelvic MR images. For the image analysis, the radiologists blinded to the examinations and clinical results.

To take into account tumor heterogeneity, the radiologists, based on pre-contrast T1-weighted images using the T2-weighted images as a guide [33], manually defined regions of interests (ROIs) along the contours of the tumor to obtain a DCE-MRI volume of interest (VOI) for each study, covering the whole lesion with exclusion of peripheral fat, artefacts and blood vessels. Also, for DW-MRI the radiologists, based on diffusion-weighted imaging with the highest  $b$  value, manually defined ROIs along the contours of the tumor to obtain a DW-MRI VOI for each study.

For each MR descriptor, the mean and the standard deviation values on the VOI were registered.

Percentage change between pre- and post-treatment was calculated as  $\Delta X = (X_{pre} - X_{post})/X_{pre}$ . ( $X$  is the generic shape descriptor.)

No image registration was applied to our data acquired. We took care to exclude from the analysis the slices where motion artefacts were visible. Moreover, a volumetric analysis for each parameter was performed, thus minimizing errors due to voxel misalignments.

#### DCE-MRI features

In order to perform SIS analysis, an OsiriX plugin has been developed by the authors [34]. Considering the segmented VOI, the maximum signal difference (MSD) and washout slope (WOS) were calculated as reported in [35]. Then for SIS analysis were evaluated the percentage change in MSD [ $\Delta MSD = (MSD_1 - MSD_2)/MSD_1 \times 100$ ], of WOS [ $\Delta WOS = (WOS_1 - WOS_2)/WOS_1 \times 100$ ] and their combination as described previously [18]. Standardized Index of Shape was given by the following linear combination:  $0.7780 \cdot \Delta MSD + 0.6157 \cdot \Delta WOS$ .

#### DWI features

For each voxel, 9 features were extracted from DWI data using the monoexponential model, the diffusion kurtosis imaging model, the intravoxel incoherent motion using

conventional biexponential fitting method and variable projection algorithm.

DWI signal decay is most commonly analyzed using the monoexponential model [23, 24]:

$$ADC = \frac{\ln\left(\frac{S_b}{S_0}\right)}{b} \quad (1)$$

where  $S_b$  is the MRI signal intensity with diffusion weighting  $b$ ,  $S_0$  is the non-diffusion-weighted signal intensity, and ADC is the apparent diffusion coefficient.

For a voxel with a large vascular fraction, the MRI data decay can deviate from a monoexponential form, in particular showing a fast decay in the range of low  $b$  values generated by the IVIM effect [23, 24]. Thus, in addition to the monoexponential model, a conventional biexponential model using Levenberg–Marquardt fitting method was used to estimate the IVIM-related parameters of pseudo-diffusivity ( $D_p$  indicated also with  $D^*$ ), perfusion fraction ( $f_p$  indicated also with  $f$ ) and tissue diffusivity ( $D_t$ ):

$$\frac{S_b}{S_0} = f_p \cdot \exp(-b \cdot D_p) + (1 - f_p) \cdot \exp(-b \cdot D_t) \quad (2)$$

Moreover, diffusion kurtosis imaging was included in the analysis in order to obtain the final fitted images [mean of diffusion coefficient (MD) and mean of diffusional kurtosis (MK)].

Multi- $b$  DW images were obtained by voxel-wise fitting using the diffusion kurtosis signal decay Eq. (3) by a two-variable linear least-squares algorithm as used in previous study [32]:

$$S(b) = S_0 \exp\left(-b \cdot D + \frac{1}{6} b^2 \cdot D^2 \cdot K\right) \quad (3)$$

In this equation,  $D$  is a corrected diffusion coefficient and  $K$  is the excess diffusion kurtosis coefficient.  $K$  describes the degree that molecular motion deviates from the perfect Gaussian distribution. When  $K$  is equal to 0,

Eq. (3) evolves into a conventional monoexponential Eq. (1):

The difference between  $D$  and ADC is that  $D$  is a corrected form of ADC for use in non-Gaussian circumstances.

The parameters of conventional DWI (ADC), IVIM ( $f_p$ ,  $D_t$ ,  $D_p$ ) using CBFM and DKI (MK and MD) were obtained from the multi- $b$  DWI data with all measured  $b$  values using the prototype post-processing software Body Diffusion Toolbox (Siemens Healthcare, Erlangen, Germany).

Moreover, for each voxel on DW, data diffusion and perfusion information were also obtained modeling DW-data using the IVIM model and using VARPRO algorithm for parameters estimation [36].

Rearranging Eq. (2) the  $S(b)/S_0 - e^{-bD_t}$  is the product of  $f$  and a nonlinear function of  $D_t$  and  $D_p$ :

$$f(D_p; D_t; b) = S(b)/S_0 - e^{-bD_t} = f(e^{-bD_p} - e^{-bD_t}) \quad (3)$$

Letting  $f(D_p; D_t; b)$  the cost functional becomes:

$$S(b)/S_0 - e^{-bD_t} = \|y - f(D_p; D_t; b)\|_2 \quad (4)$$

Therefore, a separable nonlinear least square algorithm known as variable projection (VARPRO) can be used to calculate the diffusion parameters. If we knew the estimate of the nonlinear parameters  $D_p$  and  $D_t$ , the estimate of the linear parameter  $f$  could be obtained by solving a linear least square problem:

$$f = e^{-bD_t} + y + f(D_p; D_t; b)^+ \quad (5)$$

where  $f(D_p; D_t; b)^+$  is the Moore–Penrose generalized inverse of  $f(D_p; D_t; b)$ . Therefore, a new cost functional can be constructed:

$$S(b)/S_0 - e^{-bD_t} = \|y - f(D_p; D_t; b)f(D_p; D_t; b)^+ y\| \quad (5)$$

An exhaustive description of the algorithm is beyond the scope of the present paper, and the interested reader is referred to [37]. This analysis was performed using MATLAB R2007a (The MathWorks Inc., Natick, MA).

Per each MR descriptor, the mean and the standard deviation values were registered.

### Evaluation of pathologic response

The pathologic response assessment was performed according to previously published recommendations [38, 39]. Briefly, surgical specimens containing the tumor were evaluated and scored according to tumor regression grade (TRG), as proposed by Mandard et al. [39], by an

expert pathologist who was not aware of MRI findings. Patients with a TRG 1 or 2 score were considered as responders, whereas the remaining patients (TRG 3, 4 or 5) were classified as non-responders. Patients with TRG 1 were considered with pathological complete response, while patients with TRG 2–5 were considered with incomplete pathological response [18].

### Statistical analysis

Mann–Whitney nonparametric test was performed to assess statistically significant differences between responder versus non-responder patients and between pathological complete responders versus incomplete responders. Receiver operating characteristic (ROC) curves were also used to evaluate the diagnostic performance for each parameter. Area under ROC curve (AUC) was calculated, and optimal thresholds were obtained maximizing the Youden index. Sensitivity, specificity, positive predictive value (PPV), negative predictive value (NPV) and accuracy were performed considering optimal cutoff values.

Moreover, three different neural networks were trained and used as classifiers to test the performance of a multivariate analysis of all MR-derived parameters. We used a supervised linear classifier (linear discriminant analysis), a supervised linear support vector machine and a supervised decision tree classifier. For each training set, a leave-one-out cross-validation was performed, and the best findings were registered. An exhaustive description of each classifier is beyond the scope of the present paper, and the interested reader is referred to [40–43].

Statistical analysis was performed using the mean and standard deviation values pre-treatment to assess the capability to predict pathological response before therapy, while the mean and standard deviation values post-treatment and the percentage changes were investigated to assess the SCRDS response in the preoperative phase to guide the surgery versus more conservative treatments. For each comparisons, the gold standard is the tumor regression grade obtained on surgical specimens containing the tumor.

A  $p$  value  $< 0.05$  was considered significant for all tests. All analyses were performed using Statistics Toolbox of MATLAB R2007a (The MathWorks Inc., Natick, MA).

## Results

All patients in our series had rectal adenocarcinomas. Three patients were pathologically classified as T0, 6 as T1, 20 as T2 and 5 as T3. There were 7 patients with a TRG 1, 8 with a TRG 2, 11 with a TRG 3, 8 with a TRG 4 and none with a TRG 5. Therefore, 15 patients were classified as responders and 19 as not responders by TRG. Seven patients had pathological complete response.

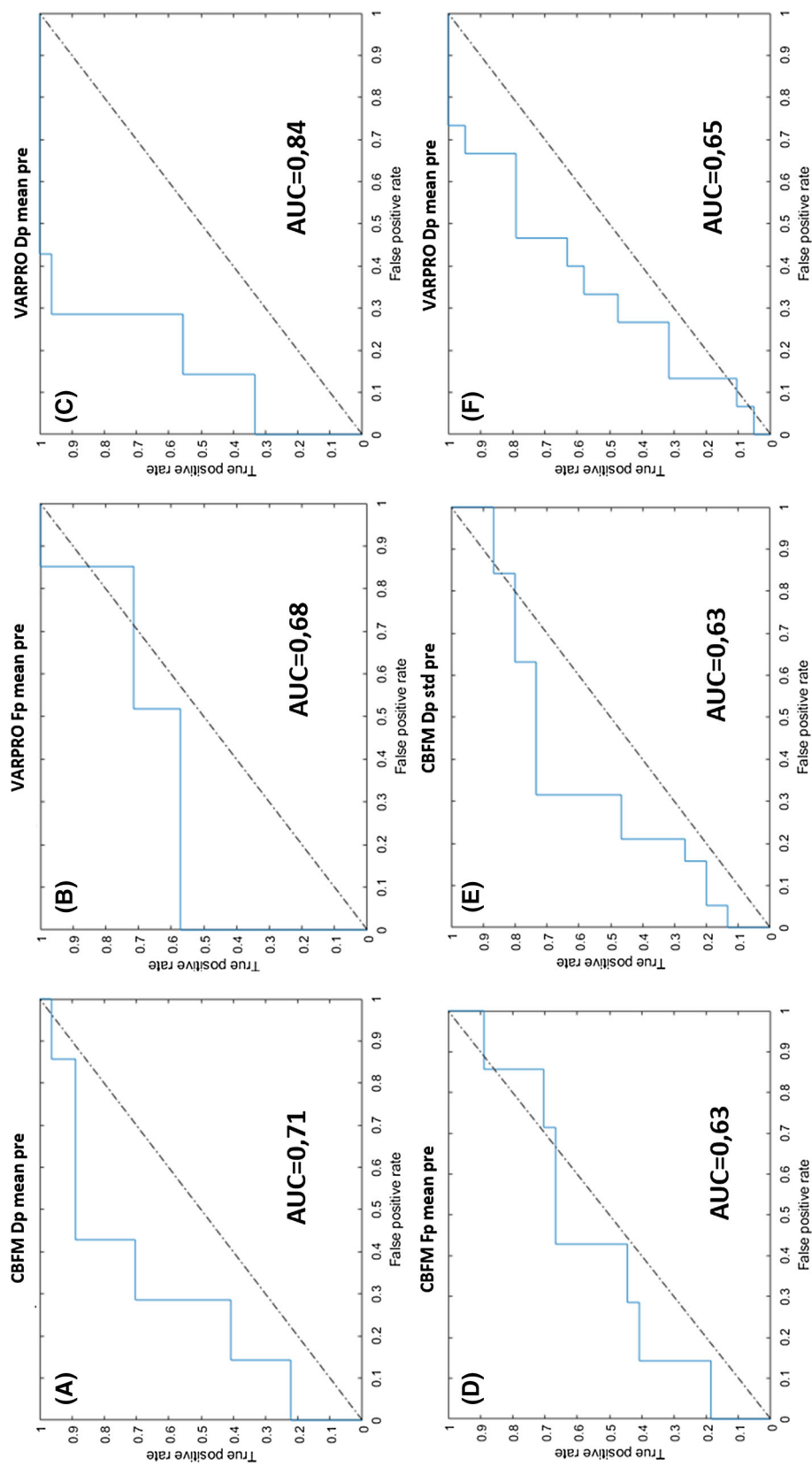


Fig. 2. ROC analysis for the best MR-derived parameters to predict pathological complete response and responder patients of the SCRDS.

**Table 3.** Diagnostic performance of the best MR-derived parameters to predict pathological complete response and responder patients of the SCRDS

	CBFM $D_p$ mean pre-treatment	VARPRO $F_p$ mean pre-treatment	VARPRO $D_p$ mean pre-treatment
To predict pathological complete response			
Cutoff	0.0145	0.6607	0.0039
Sensitivity	0.8889	0.5714	0.9630
Specificity	0.5714	1.0000	0.7143
PPV	0.8889	1.0000	0.9286
NPV	0.5714	0.9000	0.8333
Accuracy	0.8235	0.9118	0.9118
	CBFM $F_p$ mean pre-treatment	CBFM $D_p$ std pre-treatment	VARPRO $D_p$ mean pre-treatment
To predict responder patients			
Cutoff	0.2428	0.0003	0.0070
Sensitivity	0.7333	0.6842	0.7895
Specificity	0.6842	0.6667	0.5333
PPV	0.6471	0.7222	0.6818
NPV	0.7647	0.6250	0.6667
Accuracy	0.7059	0.6765	0.6765

CBFM, conventional biexponential fitting model; VARPRO, variable projection; PPV, positive predictive value; NPV, negative predictive value; std, standard deviation

Considering the high number of parameters investigated, we reported exclusively the findings for parameters that resulted statistically significant.

Mean and standard deviation values of pre-treatment CBFM  $D_p$  and mean value of VARPRO  $D_p$  pre-treatment showed statistically significant differences to predict pathological complete response. ( $p$  value at Mann–Whitney test was 0.05, 0.03 and 0.008, respectively.)

Instead, Mann–Whitney test showed statistically significant differences exclusively for SIS percentage change between responder and non-responder patients ( $p$  value  $< < 0.001$ ) and between pathological complete responders and incomplete responders after SCRDS ( $p$  value  $< < 0.001$ ).

The best results to predict pathological complete response were obtained by CBFM  $D_p$  mean value pre-treatment, VARPRO  $F_p$  mean value pre-treatment and for VARPRO  $D_p$  mean value pre-treatment (Fig. 2a–c) with area under ROC of 0.71, 0.68 and 0.84 (Table 3), respectively.

The best results to predict responders were obtained by CBFM  $F_p$  mean value pre-treatment, CBFM  $D_p$  standard deviation value pre-treatment and for VARPRO  $D_p$  mean value pre-treatment (Fig. 2d–f) with area under ROC of 0.63, 0.63 and 0.65 (Table 3), respectively.

The best results to detect after treatment complete pathological response were obtained by SIS, the percentage change in MK standard deviation and by percentage change in VARPRO  $D_p$  mean value (Fig. 3a–c) with area under ROC of 0.89, 0.70 and 0.72 (Table 4), respectively.

The best results to differentiate responders vs. non-responders after treatment were obtained by SIS, the percentage change in MK standard deviation and percentage change in VARPRO  $D_p$  mean value (Fig. 3d–f)

with area under ROC of 0.94, 0.60 and 0.65 (Table 4), respectively.

Table 5 reports the diagnostic performance of tested classifiers to predict pathological response before treatment and to assess pathological response after treatment. The best results (bold values) were obtained by a supervised decision tree with an accuracy of 88.2% to predict pathological complete response using VARPRO  $D_p$  pre-treatment mean value, ADC standard deviation value pre-treatment (Fig. 4a and b). However, these results showed a worse accuracy compared at the use of CBFM  $D_p$  mean pre-treatment, VARPRO  $F_p$  mean pre-treatment VARPRO  $D_p$  mean pre-treatment mean value alone. Instead, to predict responder patients the best results (bold values) were obtained by a supervised decision tree with an accuracy of 64.7% using CBFM IVIM  $F_p$  pre-treatment mean and standard deviation value, MK standard deviation value pre-treatment, ADC standard deviation value pre-treatment (Fig. 4c and d). However, these results showed a worse accuracy compared at the use of CBFM  $F_p$  mean pre-treatment CBFM  $D_p$  std pre-treatment VARPRO  $D_p$  mean pre-treatment.

The best results (bold values) to assess pathological complete response after SCRDS were obtained by a supervised decision tree with an accuracy of 85.3% using VARPRO  $D_p$  mean value post-treatment, ADC standard deviation value pre-treatment, MD standard deviation value post-treatment (Fig. 5a and b). Instead, low accuracy (55.9%) was reached in the assessment of responder patients after SCRDS considering the best results (bold values) by a supervised decision tree using VARPRO  $D_p$  mean value post-treatment, VARPRO  $D$  mean value pre- and post-treatment (Fig. 5c and d).

We reported representative MR images for a responder patient (TRG = 2). Figure 6 shows SIS analysis,  $\Delta$ SIS = 24.79%. Figure 7 shows ADC- and



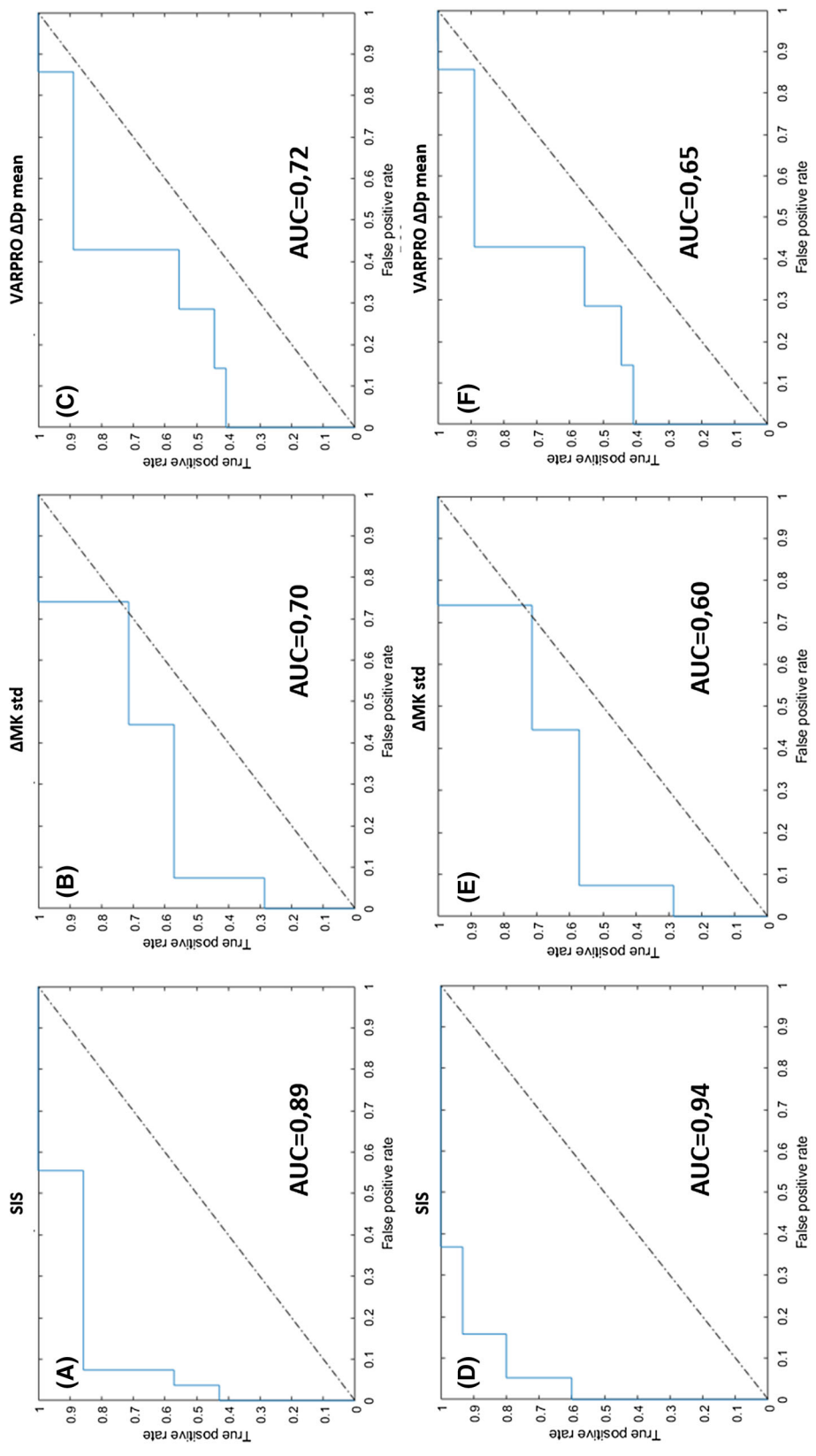


Fig. 3. ROC analysis of the best MR-derived parameters to assess pathological complete response and to detect responder patients after SCRDs.

**Table 4.** Diagnostic performance of the best MR-derived parameters to assess pathological complete response and to detect responder patients after SCRDS

	SIS	$\Delta$ MK std	VARPRO $\Delta D_p$ mean
To detect pathological complete response			
Cutoff	69.9571	60.5039	- 574.6957
Sensitivity	0.8571	0.5714	0.8889
Specificity	0.9259	0.9259	0.5714
PPV	0.7500	0.6667	0.8889
NPV	0.9615	0.8929	0.5714
Accuracy	0.9118	0.8529	0.8235
To detect responder patients			
Cutoff	- 7.7694	60.5039	- 574.6957
Sensitivity	0.9333	0.3333	0.8947
Specificity	0.8421	0.9474	0.3333
PPV	0.8235	0.8333	0.6296
NPV	0.9412	0.6429	0.7143
Accuracy	0.8824	0.6765	0.6471

CBFM, conventional biexponential fitting model; VARPRO, variable projection; PPV, negative predictive value; NPV, negative predictive value; std, standard deviation

IVIM-derived parameter maps pre-treatment (a, c, e, g) and post-treatment (b, d, f, h):  $\Delta$ ADC = - 87.25%,  $\Delta$ D = - 99.36%,  $\Delta D_p$  = 8.42%,  $\Delta f_p$  = 38.67%. Figure 8 shows DKI-derived parameters maps pre-treatment (a, c) and post-treatment (b, d):  $\Delta$ MD = - 45.79%,  $\Delta$ MK = 55.29%.

Figure 9 shows an image representative of the correlation of tumor on MR T2-weighted images with pathology specimen.

### Discussion

Recently, there has been growing interest in functional imaging modalities to increase diagnostic accuracy for therapy response assessment. These imaging modalities reflect the microstructural and metabolic proprieties of the tumor, allowing the assessment of treatment-induced changes before morphological changes are visible. DCE-MRI and DWI have emerged as powerful tools to predict and to assess neoadjuvant therapy response for rectal cancer. In fact, DCE- and DW-MR imaging after pre-operative CRT was shown to be more valuable than morphologic MR imaging to recognize pathological significant and complete response and to discriminate viable residual tumor.

The objective of this study was to determine the diagnostic performance of DCE and DW imaging for the assessment of tumor response after SCRDS in patients with LARC comparing Standardized Index of Shape (SIS) obtained by DCE-MRI and using ADC-, intravoxel incoherent motion- and DKI-derived parameters obtained from DW-MRI and their combinations. To the best of our knowledge, there are no studies in the literature focused on a comparison of DCE-MRI-, IVIM- and DKI-derived parameters and their combination to predict and to assess therapy response in locally advanced rectal cancer after SCRDS.

**Table 5.** Performance of multivariate analysis using DWI-derived parameters and neural networks

	Parameters values considered in the analysis	Training set			Decision tree			Linear classifier			Linear support vector machine					
		ACC	SEN	SPEC	PPV	NPV	ACC	SEN	SPEC	PPV	NPV	ACC	SEN	SPEC	PPV	NPV
To predict pathological complete response	Pre-treatment values	50.00	0.00	0.63	0.00	0.71	61.80	0.14	0.74	0.13	0.77	79.40	0.00	1.00	-	0.79
	ADC,DKI, CBFM IVIM															
To predict responder patients	Pre-treatment values	<b>88.20</b>	<b>0.57</b>	<b>0.96</b>	<b>0.80</b>	<b>0.90</b>	76.50	0.29	0.89	0.40	0.83	79.40	0.14	0.96	0.50	0.81
	ADC,DKI, CBFM IVIM	<b>64.70</b>	<b>0.60</b>	<b>0.68</b>	<b>0.60</b>	<b>0.68</b>	58.80	0.40	0.74	0.55	0.61	52.90	0.13	0.84	0.40	0.55
To detect pathological complete response	Pre-treatment values, post-treatment values	47.10	0.40	0.53	0.40	0.53	44.10	0.20	0.63	0.30	0.50	47.10	0.13	0.74	0.29	0.52
	ADC,DKI, VARPRO IVIM	52.90	0.00	0.67	0.00	0.72	61.80	0.29	0.70	0.20	0.79	79.40	0.00	1.00	-	0.79
To detect responder patients	Pre-treatment values, post-treatment values	<b>85.30</b>	<b>0.57</b>	<b>0.93</b>	<b>0.67</b>	<b>0.89</b>	70.60	0.43	0.78	0.33	0.84	82.40	0.14	1.00	1.00	0.82
	ADC,DKI, CBFM IVIM	44.10	0.40	0.47	0.38	0.50	52.90	0.60	0.47	0.47	0.60	52.90	0.20	0.79	0.43	0.56
	Pre-treatment values, post-treatment values	<b>55.90</b>	<b>0.53</b>	<b>0.58</b>	<b>0.50</b>	<b>0.61</b>	41.20	0.27	0.53	0.31	0.48	47.10	0.13	0.74	0.29	0.52
	ADC,DKI, VARPRO															

CBFM, conventional biexponential fitting model; VARPRO, variable projection; SEN, sensitivity; SPEC, specificity; PPV, positive predictive value; NPV, negative predictive value; std, standard deviation

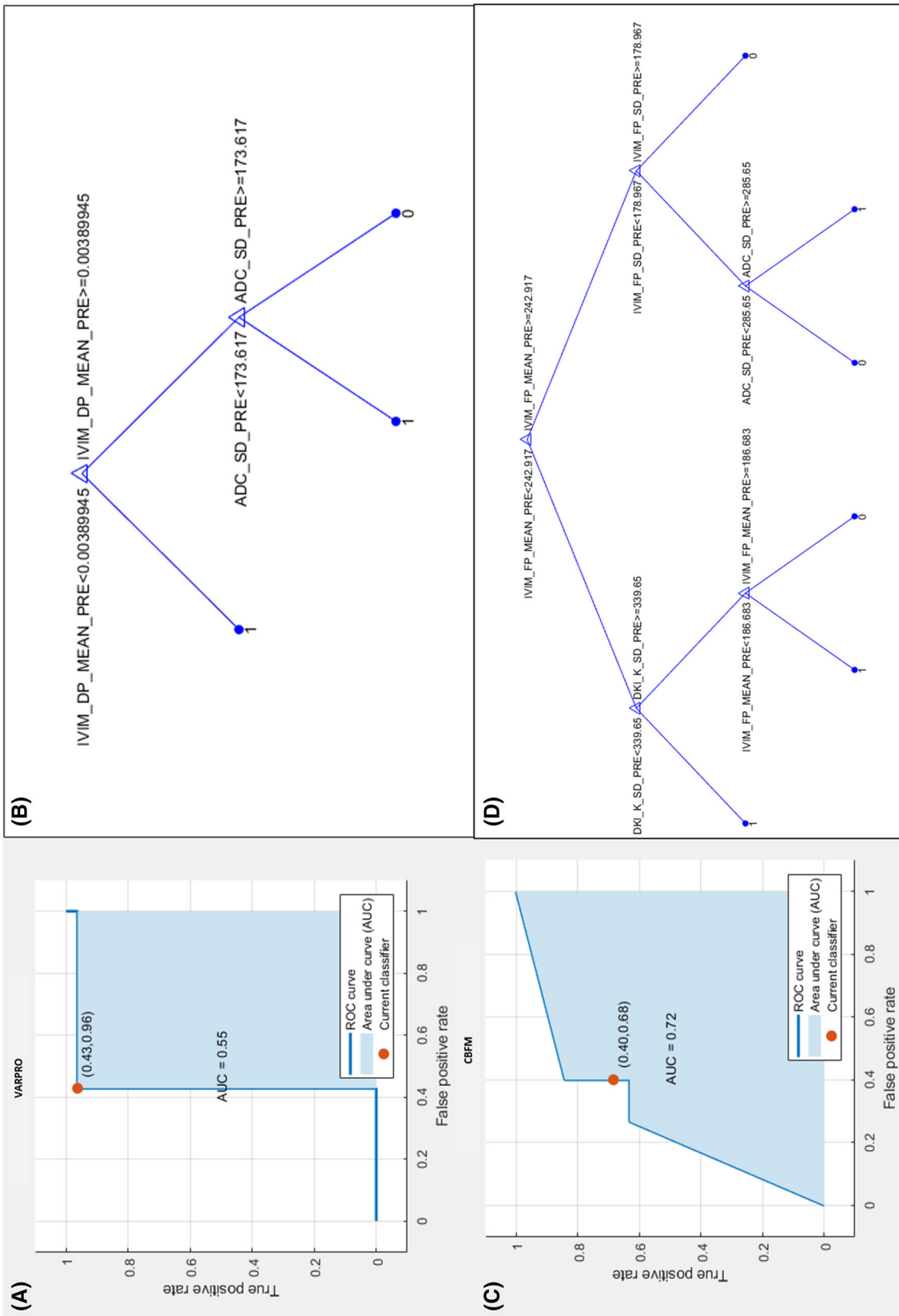


Fig. 4. ROC curve and the best decision tree to predict pathological complete response using VARPRO  $D_p$  pre-treatment mean value, ADC standard deviation value pre-treatment (Fig. 4a and b) and the best decision tree to predict responder patients using CBFM  $IVIM F_p$  pre-treatment mean and standard deviation values, MK standard deviation value pre-treatment, ADC standard deviation value pre-treatment (Fig. 3c and d).

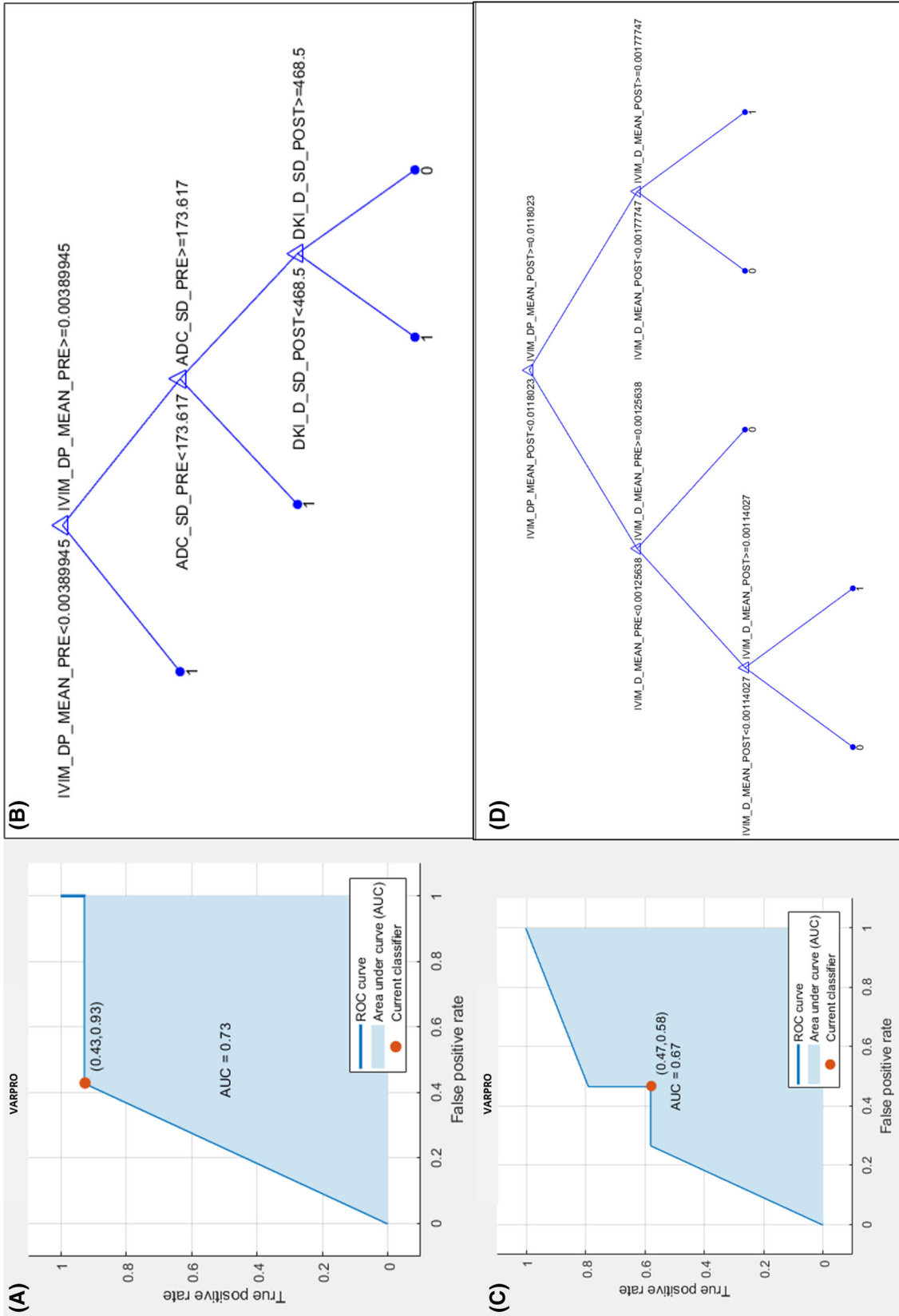


Fig. 5. Figure shows the ROC curve and the best decision tree to assess pathological complete response after SCRDS using VARPRO  $D_p$  mean value post-treatment, ADC standard deviation value pre-treatment, MD standard deviation value post-treatment (Fig. 4a and b) and the ROC curve and the best decision tree to assess responder patients after SCRDS using VARPRO  $D_p$  mean value pre- and post-treatment (Fig. 4c and d).

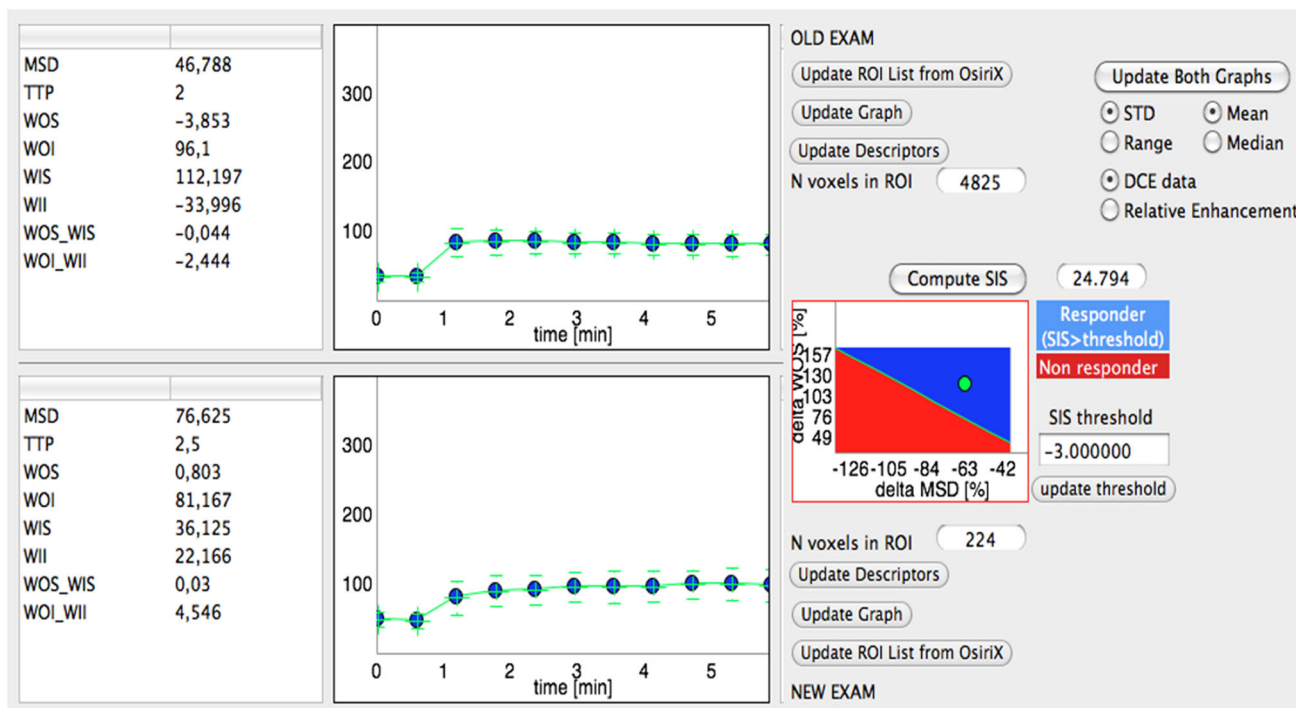
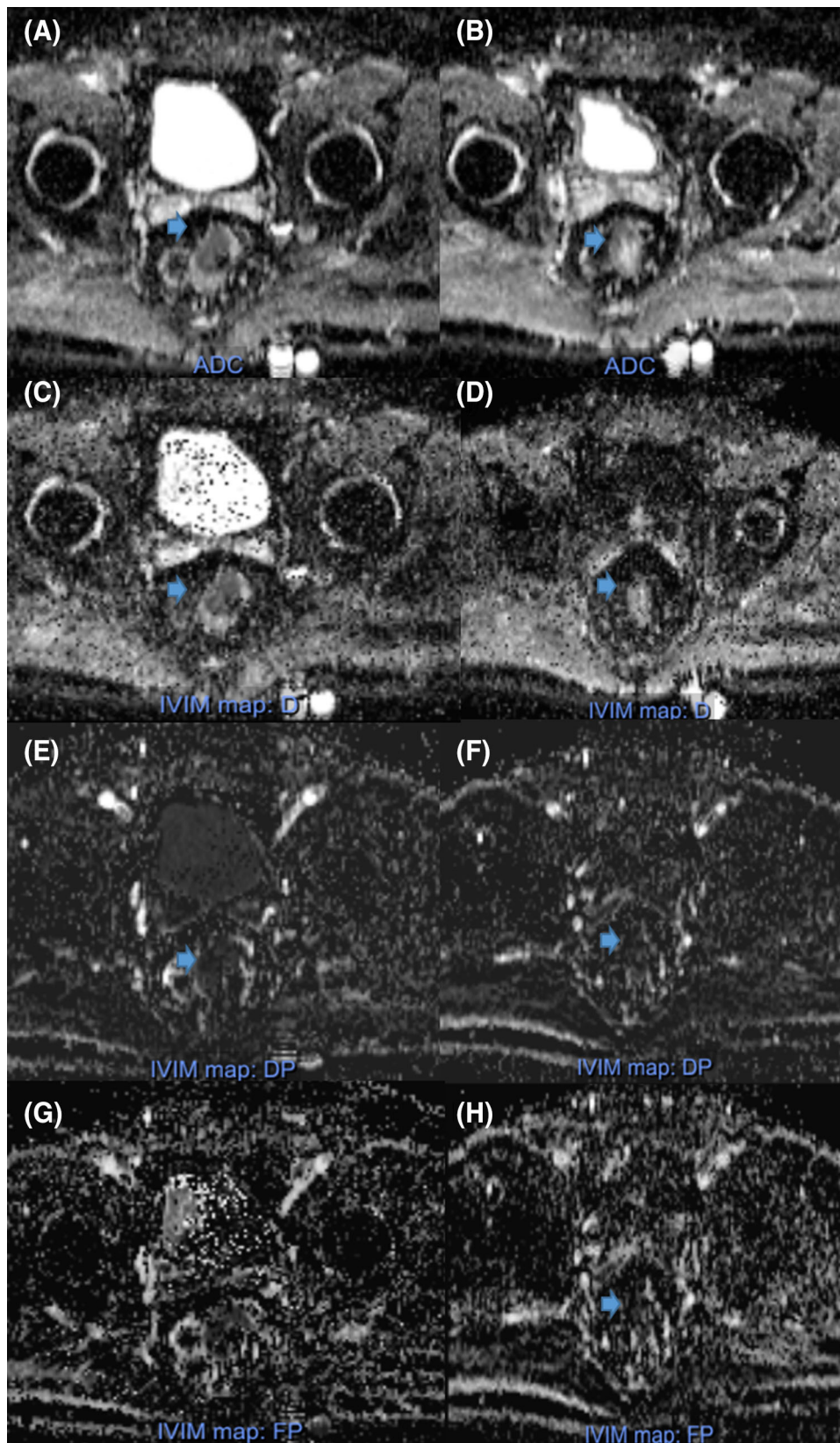


Fig. 6. Figure shows SIS analysis for a responder patients: TRG 2 and  $\Delta$ SIS = 24.79%.

There are many studies that evaluate the single modality, DCE or DWI, in preoperative long CRT assessment [18–21, 44–46]. In our previous studies [18], we demonstrated the ability of DCE-MRI using the Standardized Index of Shape to discriminate significant responders and pathological complete tumor response after preoperative CRT in LARC with a good accuracy also when compared to FDG-PET examinations [47]. Several studies demonstrated the role of diffusion-weighted imaging in LARC for early and late assessment of therapy response [44–46], and several studies evaluated the use of IVIM to elaborate DW-data in different kind of tumors [27–30, 48]. Choi et al. [44] demonstrated that ADC values have significant difference between pathological complete response and non-pathological complete response groups, demonstrating the utility of the ADC value as a quantitative objective biomarker in rectal cancer. Moreover, there are some studies with the aim to assess tumor response after SCR using metabolic change evaluations by FDG-PET with contrasting results [49–52]. In another study [19], we assessed SIS- and IVIM-derived parameters in LARC after SCRDS demonstrating that SIS obtained the best parameter to discriminate responders by non-responders (sensitivity 94%, specificity 84%, accuracy 89%, cutoff value =  $-7.8\%$ ) and the best diagnostic performance also to discriminate pCR (sensitivity 86%, specificity 89%, accuracy 89%, cutoff value =  $68.2\%$ ) and that no accuracy increase was obtained combining linearly each possible parameters couple or combining all functional MR-derived parameters compared to SIS alone.

Only few researches have evaluated the role of DKI for assessing treatment response of neoadjuvant chemoradiotherapy in LARC [53, 54]. Yu et al. [53] evaluated the feasibility and value of DKI in assessing treatment response to neoadjuvant CRT in LARC. In their study, histogram analysis of imaging indices (MD, MK, ADC) was performed and evaluated on 41 patients. The results by Yu et al. [53] suggested that the percentage change in MD provides high diagnostic performance for assessing treatment response. For pre-CRT parameters, histogram indices medians and 10th percentiles of pre-MD correlated statistically with TRG scores, providing a good performance for evaluating treatment to neoadjuvant CRT. Hu et al. assessed the value of DKI in evaluating pathological complete response to neoadjuvant CRT compared to conventional DWI [54] using a proper DKI scan protocol with  $b$  values of 0, 700, 1400 and 2000. They enrolled 56 patients with LARC that underwent MRI before and after CRT. They showed that among 56 rectal lesions (pCR,  $n = 14$ ; non-pCR,  $n = 42$ ), the MK pre- and MK post-values were much lower for pCR patients than for non-pCR patients. The ADC post and ADC percentage change was significantly higher for pCR patients than for non-pCR. The MK post showed relatively high sensitivity and high specificity in comparison with other parameters. Our findings showed that mean and standard deviation values pre-treatment of CBFM  $D_p$  and mean value of VARPRO  $D_p$  pre-treatment showed statistically significant differences between pathological complete responders and incomplete responders ( $p$  value at Mann–Whitney test was



**Fig. 7.** Figure shows ADC- and IVIM-derived parameters maps pre-treatment (**A, C, E, G**) and post-treatment (**B, D, F, H**) for a responder patients (TRG 2): ADC (**A**) and (**B**),  $D$  (**C**) and (**D**),  $D_p$  (**E**) and (**F**),  $f_p$  (**G**) and (**H**).

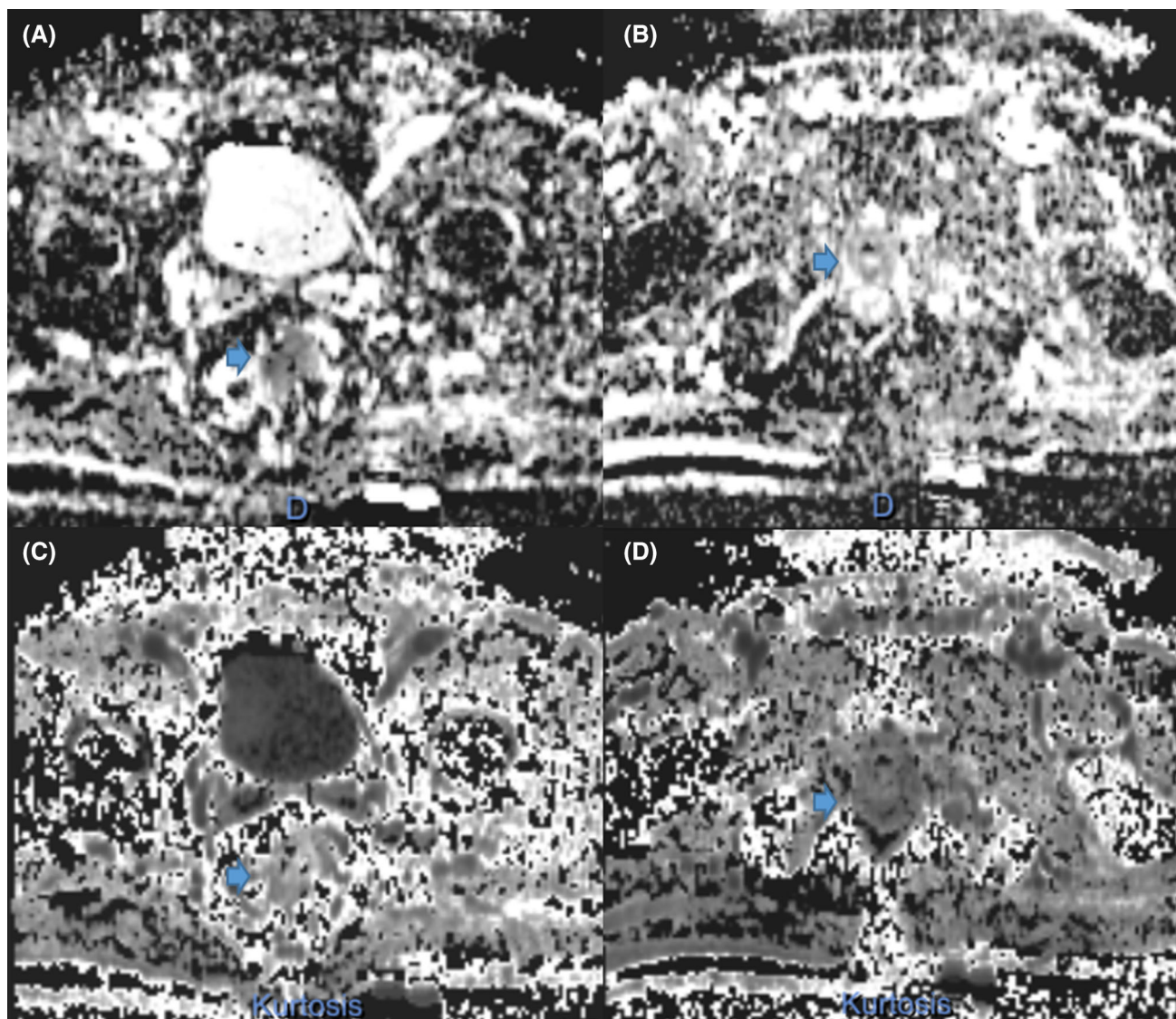


**Fig. 8.** Figure shows DKI-derived parameters maps pre-treatment (A), (C) and post-treatment (B), (D) for a responder patients (TRG 2): MD (A) and (B), MK (C) and (D).

0.05, 0.03 and 0.008, respectively), while exclusively SIS percentage change showed significant differences between responder and non-responder patients after SCRDS ( $p$  value  $\ll 0.001$ ) and to assess pathological complete response after SCRDS ( $p$  value  $\ll 0.001$ ).

The best results to predict pathological complete response were obtained by VARPRO Fp mean value pre-treatment with area under ROC of 0.84, a sensitivity of 96.4%, a specificity of 71.4%, a positive predictive value of 92.9%, a negative predictive value of 83.3% and an accuracy of 91.2%. The best results to assess post-treatment complete pathological response were obtained by SIS with an area under ROC of 0.89, a sensitivity of 85.7%, a specificity of 92.6%, a positive predictive value of 75.0%, a negative predictive value of 96.1% and an accuracy of 91.2%. Moreover, the best results to differentiate post-treatment responders by non-responders

were obtained by SIS with an area under ROC of 0.94, a sensitivity of 93.3%, a specificity of 84.2%, a positive predictive value of 82.4%, a negative predictive value of 94.1% and an accuracy of 88.2%.

These results take the conclusion that DWI-derived parameters including pseudo-diffusion coefficient and perfusion fraction have a great potential to predict therapy response and then patient outcome before treatment in LARC, while SIS is the best parameter to assess pathological response after treatment to guide surgery.

Promising results were obtained using a decision tree tested with all ADC-, IVIM- and DKI-derived parameters. A high accuracy was reached for the assessment of pathological complete response after SCRDS in LARC. The best results were obtained with a supervised decision tree with an accuracy of 85.3% to assess pathological

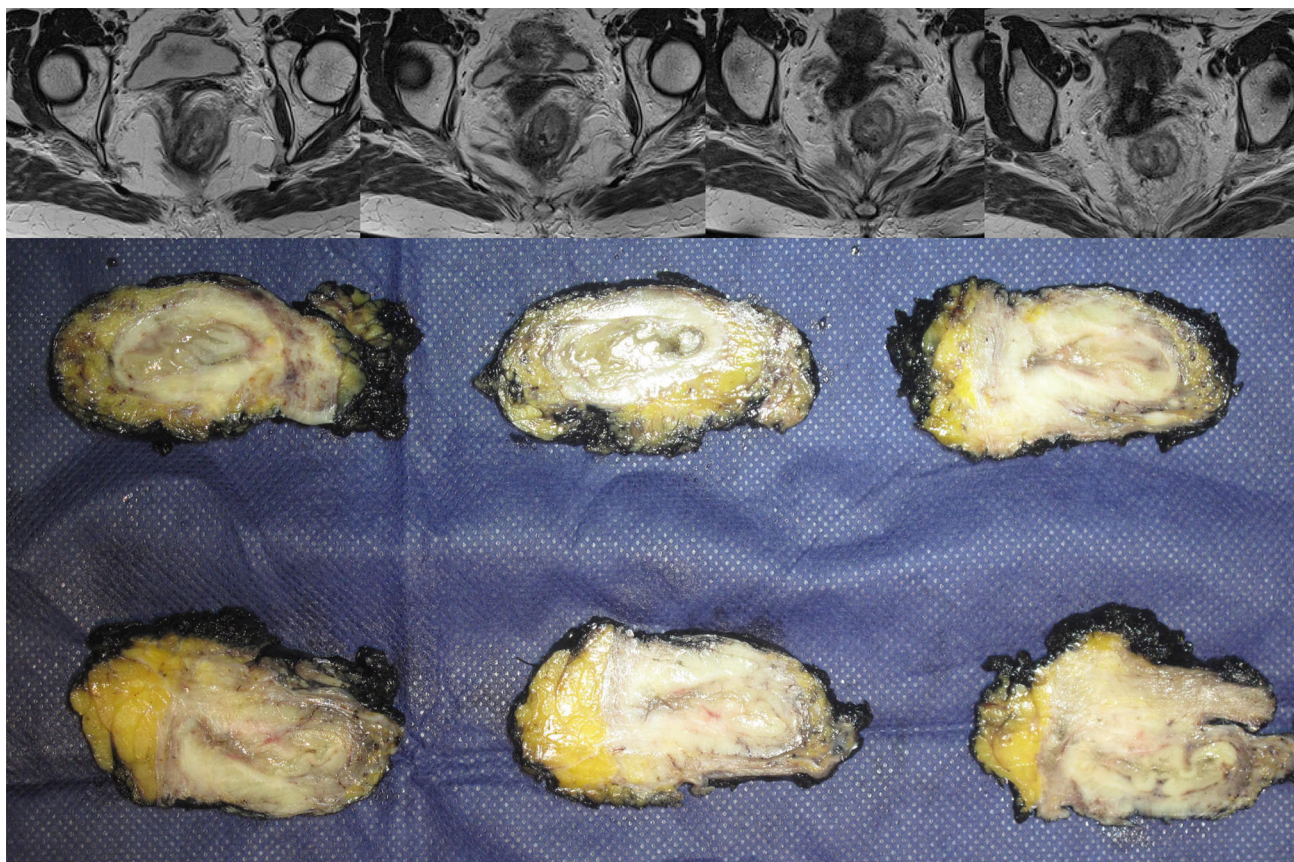


**Fig. 9.** A representative image that shows the correlation of tumor on MR T2-weighted images with the pathology specimens.

complete response after SCRDS using VARPRO  $D_p$  mean value post-treatment, ADC standard deviation value pre-treatment, MD standard deviation value post-treatment. However, SIS alone showed a major accuracy. In any case, these results could be interesting when contrast agent administration was contraindicated and DCE-MRI cannot be performed.

Some potential limitations deserve a special consideration: two radiologists evaluated the MR images by consensus and in a single session per patient so that the intraobserver variability was not assessed. The calculation of DKI parameters may be suboptimal for the use of an acquisition protocol with  $800 \text{ m/s}^2$  as a maximum  $b$  value. A more extensive patient panel would probably strengthen the power of this study in SCR therapy assessment. A reproducibility analysis of MR-derived parameters was not performed; however, the use of mean values for each DCE and DW parameters extracted by volume of interest allows to obtain more robust measures.

## Conclusions

In conclusion, perfusion fraction derived by IVIM model using a more sophisticated fitting approach compared to convention biexponential fitting using Levenberg–Mar-

quardt had high accuracy to predict positive therapy response after SCR. On the other side, SIS is an encouraging DCE-MRI angiogenic biomarker to assess preoperative treatment response after SCR with delayed surgery, and it permits to discriminate pathological complete response allowing direct surgery for tailored and conservative treatment. Furthermore, an important prognostic role was obtained by perfusion fraction mean value pre-treatment and by a decision tree composed by VARPRO  $D_p$  mean value post-treatment, ADC standard deviation value pre-treatment, MD standard deviation value post-treatment in order to assess pathological complete response.

**Acknowledgements** Writing/editorial support in the preparation of this manuscript was provided by Di Giovanni Manuela, University of Technology, Sydney, Australia.

**Author contributions** All authors contributed to this work for patient's enrollment, diagnostic and therapeutic procedures. RF performed image post-processing, statistical analysis and manuscript editing. **Data availability** All data were present in the text of manuscript.

**Compliance with ethical standards**

**Funding** No funding.

**Conflict of interest** Each author declares that has no conflict of



interest. Exclusively Robert Grimm (Robert.grimm@siemens.com) is an employee of Siemens Healthcare for development of the MR Body Diffusion Toolbox, a post-processing software to calculate IVIM and Kurtosis maps.

**Ethics approval and consent to participate** All procedures performed in studies involving human participants were in accordance with the ethical standards of the institutional and/or national research committee and with the 1964 Helsinki Declaration and its later amendments or comparable ethical standards. Informed consent was obtained from all individual participants included in the study.

**Consent for publication** Consent was obtained from all individual participants included in the study.

## References

- Avallone A, Aloj L, Delrio P, et al. (2013) Multidisciplinary approach to rectal cancer: are we ready for selective treatment strategies? *Anticancer Agents Med Chem* 13(6):852–860
- Avallone A, Delrio P, Guida C, et al. (2006) Biweekly oxaliplatin, raltitrexed, 5-fluorouracil and folinic acid combination chemotherapy during preoperative radiation therapy for locally advanced rectal cancer: a phase I-II study. *Br J Cancer* 94(12):1809–1815
- Delrio P, Avallone A, Guida C, et al. (2005) Multidisciplinary approach to locally advanced rectal cancer: results of a single institution trial. *Suppl Tumori* 4(3):S8.
- Zhou ZR, Liu SX, Zhang TS, et al. (2014) Short-course preoperative radiotherapy with immediate surgery versus long-course chemoradiation with delayed surgery in the treatment of rectal cancer: a systematic review and meta-analysis. *Surg Oncol* 23(4):211–221
- Latkauskas T, Pauzas H, Gineikiene I, et al. (2012) Initial results of a randomized controlled trial comparing clinical and pathological downstaging of rectal cancer after preoperative short-course radiotherapy or long-term chemoradiotherapy, both with delayed surgery. *Colorectal Dis* 14(3):294–298
- Bujko K, Kolodziejczyk M (2008) The 5 × 5 Gy with delayed surgery in non-resectable rectal cancer: a new treatment option. *Radiother Oncol* 87(3):311–313
- Beppu N, Matsubara N, Noda M, et al. (2015) Short-course radiotherapy with delayed surgery versus conventional chemoradiotherapy: a comparison of the short- and long-term outcomes in patients with T3 rectal cancer. *Surgery* 158(1):225–235.
- Pettersson D, Holm T, Iversen H, et al. (2012) Preoperative short-course radiotherapy with delayed surgery in primary rectal cancer. *Br J Surg* 99(4):577–583
- Pettersson D, Lörin E, Holm T, et al. (2015) Tumour regression in the randomized Stockholm III trial of radiotherapy regimens for rectal cancer. *Br J Surg* 102(8):972–978; discussion 8.
- Radu C, Berglund A, Pahlman L, Glimelius B (2008) Short-course preoperative radiotherapy with delayed surgery in rectal cancer—a retrospective study. *Radiother Oncol* 87(3):343–349
- Hatfield P, Hingorani M, Radhakrishna G, et al. (2009) Short-course radiotherapy, with elective delay prior to surgery, in patients with unresectable rectal cancer who have poor performance status or significant co-morbidity. *Radiother Oncol* 92(2):210–214
- Valentini V, Glimelius B, Haustermans K, et al. (2014) EURECCA consensus conference highlights about rectal cancer clinical management: the radiation oncologist's expert review. *Radiother Oncol* 110(1):195–198
- Avallone A, Piccirillo MC, Delrio P, et al. (2014) Phase 1/2 study of valproic acid and short-course radiotherapy plus capecitabine as preoperative treatment in low-moderate risk rectal cancer-V-shoRT-R3 (Valproic acid—short Radiotherapy—rectum 3rd trial). *BMC Cancer* 24(14):875
- Heo SH, Kim JW, Shin SS, Jeong YY, Kang H-K (2014) Multimodal imaging evaluation in staging of rectal cancer. *World J Gastroenterol* 20(15):4244–4255
- Fusco R, Sansone M, Petrillo M, et al. (2004) Role of magnetic resonance imaging in locally advanced rectal cancer, colorectal cancer—surgery, diagnostics and treatment. InTech. <https://doi.org/10.5772/56831>.
- Beets-Tan RG, Beets GL (2004) Rectal cancer: review with emphasis on MR imaging. *Radiology* 232(2):335–346
- Leach MO, Brindle KM, Evelhoch JL, et al. (2005) The assessment of antiangiogenic and antivascular therapies in early-stage clinical trials using magnetic resonance imaging: issues and recommendations. *Br J Cancer* 92(9):1599–1610
- Petrillo A, Fusco R, Petrillo M, et al. (2015) Standardized Index of Shape (SIS): a quantitative DCE-MRI parameter to discriminate responders by non-responders after neoadjuvant therapy in LARC. *Eur Radiol*
- Petrillo M, Fusco R, Catalano O, et al. (2015) MRI for assessing response to neoadjuvant therapy in locally advanced rectal cancer using DCE-MR and DW-MR data sets: a preliminary report. *Biomed Res Int* 2015:514740
- Beets-Tan RG, Beets GL (2014) MRI for assessing and predicting response to neoadjuvant treatment in rectal cancer. *Nat Rev Gastroenterol Hepatol* 11(8):480–488
- Phongkitkarun S, Tohmad U, Larbcharoensub N, et al. (2016) DCE-MRI-derived parameters as predictors of response to neoadjuvant chemoradiation treatment of rectal carcinoma. *J Med Assoc Thai* 99(3):338–347
- Petrillo A, Fusco R, Granata V, et al. (2017) MR imaging perfusion and diffusion analysis to assess preoperative Short Course Radiotherapy response in locally advanced rectal cancer: Standardized Index of Shape by DCE-MRI and intravoxel incoherent motion-derived parameters by DW-MRI. *Med Oncol* 34(12):198
- Le Bihan D, Breton E, Lallemand D, et al. (1988) Separation of diffusion and perfusion in intravoxel incoherent motion MR imaging. *Radiology* 168(2):497–505
- Le Bihan D, Breton E, Lallemand D, et al. (1986) MR imaging of intravoxel incoherent motions: application to diffusion and perfusion in neurologic disorders. *Radiology* 161(2):401–407
- Oto A, Yang C, Kayhan A, et al. (2011) Diffusion-weighted and dynamic contrast-enhanced MRI of prostate cancer: correlation of quantitative MR parameters with Gleason score and tumor angiogenesis. *AJR Am J Roentgenol* 197(6):1382–1390
- Curvo-Semedo L, Lambregts DM, Maas M, et al. (2011) Rectal cancer: assessment of complete response to preoperative combined radiation therapy with chemotherapy—conventional MR volumetry versus diffusion-weighted MR imaging. *Radiology* 260(3):734–743
- Luciani A, Vignaud A, Cavet M, et al. (2008) Liver cirrhosis: intravoxel incoherent motion MR imaging—pilot study. *Radiology* 249(3):891–899
- Wirestam R, Borg M, Brockstedt S, et al. (2001) Perfusion-related parameters in intravoxel incoherent motion MR imaging compared with CBV and CBF measured by dynamic susceptibility contrast MR technique. *Acta Radiol* 42(2):123–128
- Granata V, Fusco R, Catalano O, et al. (2016) Intravoxel incoherent motion (IVIM) in diffusion-weighted imaging (DWI) for Hepatocellular carcinoma: correlation with histologic grade. *Oncotarget* 7(48):79357–79364
- Granata V, Fusco R, Catalano O, et al. (2015) Early assessment of colorectal cancer patients with liver metastases treated with antiangiogenic drugs: the role of intravoxel incoherent motion in diffusion-weighted imaging. *PLoS ONE* 10(11):e0142876
- Koh DM, Collins DJ, Orton MR (2011) Intravoxel incoherent motion in body diffusion-weighted MRI: reality and challenges. *AJR Am J Roentgenol* 196(6):1351–1361
- Jensen JH, Helpert JA (2010) MRI quantification of non-Gaussian water diffusion by kurtosis analysis. *NMR Biomed* 23:698–710
- Dresen RC, Beets GL, Rutten HJ, et al. (2009) Locally advanced rectal cancer: MR imaging for restaging after neoadjuvant radiation therapy with concomitant chemotherapy. Part I. Are we able to predict tumor confined to the rectal wall? *Radiology* 252(1):81–91
- SIS Tool by Antonella Petrillo available requiring at an.petrillo@istitutotumori.na.it
- Fusco R, Petrillo A, Petrillo M, Sansone M (2013) Use of tracer kinetic models for selection of semi-quantitative features for DCE-MRI data classification. *Appl Magn Reson* 44(11):1311–1324
- Fusco R, Sansone M, Petrillo A (2017) A comparison of fitting algorithms for diffusion-weighted MRI data analysis using an intravoxel incoherent motion model. *MAGMA* 30(2):113–120
- Seber GAF, Wild CJ (1989) *Nonlinear regression*. New York: Wiley

38. Andreola S, Leo E, Belli F, et al. (2001) Adenocarcinoma of the lower third of the rectum surgically treated with a <10-mm distal clearance: preliminary results in 35 N0 patients. *Ann Surg Oncol* 8(7):611–615
39. Mandard AM, Dalibard F, Mandard JC, et al. (1994) Pathologic assessment of tumor regression after preoperative chemoradiotherapy of esophageal carcinoma. Clinicopathologic correlations. *Cancer* 73(11):2680–2686
40. Fukunaga K (1990) *Introduction to statistical pattern recognition*. Cambridge: Academic Press
41. Duda RO, Hart PE, Stork DG (2001) *Pattern classification*. New York: Wiley
42. Theodoridis S, Koutroumbas K (2003) *Pattern recognition*. Cambridge: Academic Press
43. Fusco R, Sansone M, Filice S, et al. (2016) Pattern recognition approaches for breast cancer DCE-MRI classification: a systematic review. *J Med Biol Eng* 36(4):449–459
44. Choi MH, Oh SN, Rha SE, et al. (2015) Diffusion-weighted imaging: apparent diffusion coefficient histogram analysis for detecting pathologic complete response to chemoradiotherapy in locally advanced rectal cancer. *J Magn Reson Imaging*. <https://doi.org/10.1002/jmri.25117>
45. Doi H, Beppu N, Kato T, et al. (2015) Diffusion-weighted magnetic resonance imaging for prediction of tumor response to neoadjuvant chemoradiotherapy using irinotecan plus S-1 for rectal cancer. *Mol Clin Oncol* 3(5):1129–1134
46. Nougaret S, Vargas HA, Lakhman Y, et al. (2016) Intravoxel incoherent motion-derived histogram metrics for assessment of response after combined chemotherapy and radiation therapy in rectal cancer: initial experience and comparison between single-section and volumetric analyses. *Radiology* 280(2):446–454
47. Petrillo A, Fusco R, Petrillo M, et al. (2017) Standardized Index of Shape (DCE-MRI) and standardized uptake value (PET/CT): two quantitative approaches to discriminate chemo-radiotherapy locally advanced rectal cancer responders under a functional profile. *Oncotarget* 8(5):8143–8153
48. Iima M, Le Bihan D (2016) Clinical intravoxel incoherent motion and diffusion MR imaging: past, present, and future. *Radiology* 278(1):13–32
49. Rega D, Pecori B, Scala D, et al. (2016) Evaluation of tumor response after short-course radiotherapy and delayed surgery for rectal cancer. *PLoS ONE* 11(8):e0160732
50. Pecori B, Lastoria S, Caracò C, et al. (2017) Sequential PET/CT with [18F]-FDG predicts pathological tumor response to preoperative short course radiotherapy with delayed surgery in patients with locally advanced rectal cancer using logistic regression analysis. *PLoS ONE* 12(1):e0169462
51. Siegel R, Dresel S, Koswig S, et al. (2008) Response to preoperative short-course radiotherapy in locally advanced rectal cancer: value of f-fluorodeoxyglucose positron emission tomography. *Onkologie* 31(4):166–172
52. Janssen MH, Ollers MC, van Stiphout RG, et al. (2010) Evaluation of early metabolic responses in rectal cancer during combined radiochemotherapy or radiotherapy alone: sequential FDG-PET-CT findings. *Radiother Oncol* 94(2):151–155
53. Yu J, Xu Q, Song JC, et al. (2017) The value of diffusion kurtosis magnetic resonance imaging for assessing treatment response of neoadjuvant chemoradiotherapy in locally advanced rectal cancer. *Eur Radiol* 27(5):1848–1857
54. Hu F, Tang W, Sun Y, et al. (2017) The value of diffusion kurtosis imaging in assessing pathological complete response to neoadjuvant chemoradiation therapy in rectal cancer: a comparison with conventional diffusion-weighted imaging. *Oncotarget* 8(43):75597–75606